WELDING OF NICKEL BASE SUPERALLOY SINGLE CRYSTALS

S. A. David
J. M. Vitek
S. S. Babu
Oak Ridge National Laboratory
1, Bethel Valley Road
Oak Ridge, TN 37831-6095

WELDING OF NICKEL BASE SUPERALLOY SINGLE CRYSTALS

S. A. David
J. M. Vitek
S. S. Babu
Oak Ridge National Laboratory
1, Bethel Valley Road
Oak Ridge, TN 37831-6095

Abstract

Oak Ridge National Laboratory has an ongoing research program to understand the weldability and microstructure evolution in single crystal and directionally solidified nickel base superalloys. This paper will present the results from an investigation of single-crystal PWA-1480 alloys. Welds were produced over a range of welding conditions and orientations using electron beam and laser beam welding processes. Both electron and laser beam welds contained extensive fusion zone cracking, and the cracks were identified as solidification cracks, *i.e.*, hot cracks. Crack free welds could be made over a very narrow range of welding conditions with preheat. The single-crystal welds contained misoriented stray grains, which play a critical role in the promotion of hot cracks in the welds. The origin of these grains is explained in terms of constitutional supercooling and the growth conditions. Detailed atom probe field ion microanalysis was carried out to determine the γ/γ' compositions and the segregation at the γ/γ' interface. The implications of the above results on the performance of welds will be discussed.

Introduction

During the last three decades, significant breakthroughs have taken place in alloy design and processing in order to meet the increasing demands on turbine airfoils, which operate at high temperatures (1-4). These breakthroughs include the development of directionally solidified alloys containing a series of columnar grains as well as single-crystal alloys. During the past two decades, single-crystal nickel-base superalloys have been studied extensively and are currently being used in gas turbine engines as turbine blades and vanes. It is anticipated that superalloy single crystals will eventually find their way into land-based gas turbines thereby extending the life and

efficiency of these engines. The high replacement costs of gas-turbine blades and vanes have necessitated the repair of aircraft gas-turbine engine components, and welding techniques for the repair of these components have been accepted as both an economical and viable alternative to the replacement of expensive components (5-8). Poor strength of the welded region and poor weldability of nickel-base superalloys have, however, remained critical issues; these issues are even more important for single-crystal turbine blades. Recently, significant advances have been made in understanding the development of microstructures in single-crystal weld (9-12).

This paper describes the results of welding, weldability, and microstructural development studies carried out on a nickel-base superalloy PWA-1480 single crystal. PWA-1480 is the first single-crystal turbine-airfoil alloy produced commercially. A detailed analysis of the microstructural features in welds made on single-crystal discs of PWA-1480 is described in another paper (13).

Alloys and Welding

Single crystals of the PWA-1480 alloy were obtained from Pratt and Whitney, United Technologies. They were in the form of rods 12 cm long and 1.5 cm in diameter. The nominal composition of the alloy in wt % was 10 Cr, 5 Co, 12 Ta, 4 W, 5 Al, 1.5 Ti, and the balance Ni. Single-crystal specimens used in making the full-penetration welds were in the form of discs approximately 1.5 cm in diameter and 0.3 cm thick. These discs were cut from the as-grown single-crystal rods using electric-spark erosion and were subsequently mechanically polished and then electropolished. Before sectioning from the as-grown crystal, the specimens were carefully oriented by means of the Laue back-reflection X-ray technique.

Electron beam (EB) and laser welds were made on these single crystals along unique crystallographic directions. EB welds were made in a flat position with a 15-kW Leybold Heraeus EB welding machine, using 100-kV accelerating voltage, 3- to 13-mA beam current, and welding speeds ranging from 4.2 to 42 mm/s. Laser welds were made using a pulsed Nd:YAG laser (Raytheon Model SS-500) capable of delivering an average power of 400 W. Pulse lengths of 1 to 3 ms over a power range of 90 to 240 W were used. The pulse rate ranged from 20 to 200 s^{-1}. Some EB and laser welds were produced with a preheat of 500°C. For EB welds, preheat was applied with a defocused beam. For laser welds, a gas torch was used for preheating. Because of the single-crystal specimen size limitations, conventional welding processes, such as gas tungsten arc (GTA) welding, were not investigated. Detailed microstructural analysis was performed using conventional metallographic, electron microscopy (scanning and transmission) and atom probe field ion microscopy techniques. For details see reference 14. The results of weldability and microstructural details are summarized below.

EB Welding

PWA-1480 discs were EB welded along the [100] and [110] directions in the plane of (100) at various welding speeds ranging from 4.2 to 42 mm/s. For the entire range of welding speeds investigated, the welds showed a severe cracking tendency. Both longitudinal and transverse cracks were observed in the welded specimens. Figure 1 shows the extent of cracking observed in a typical weld.

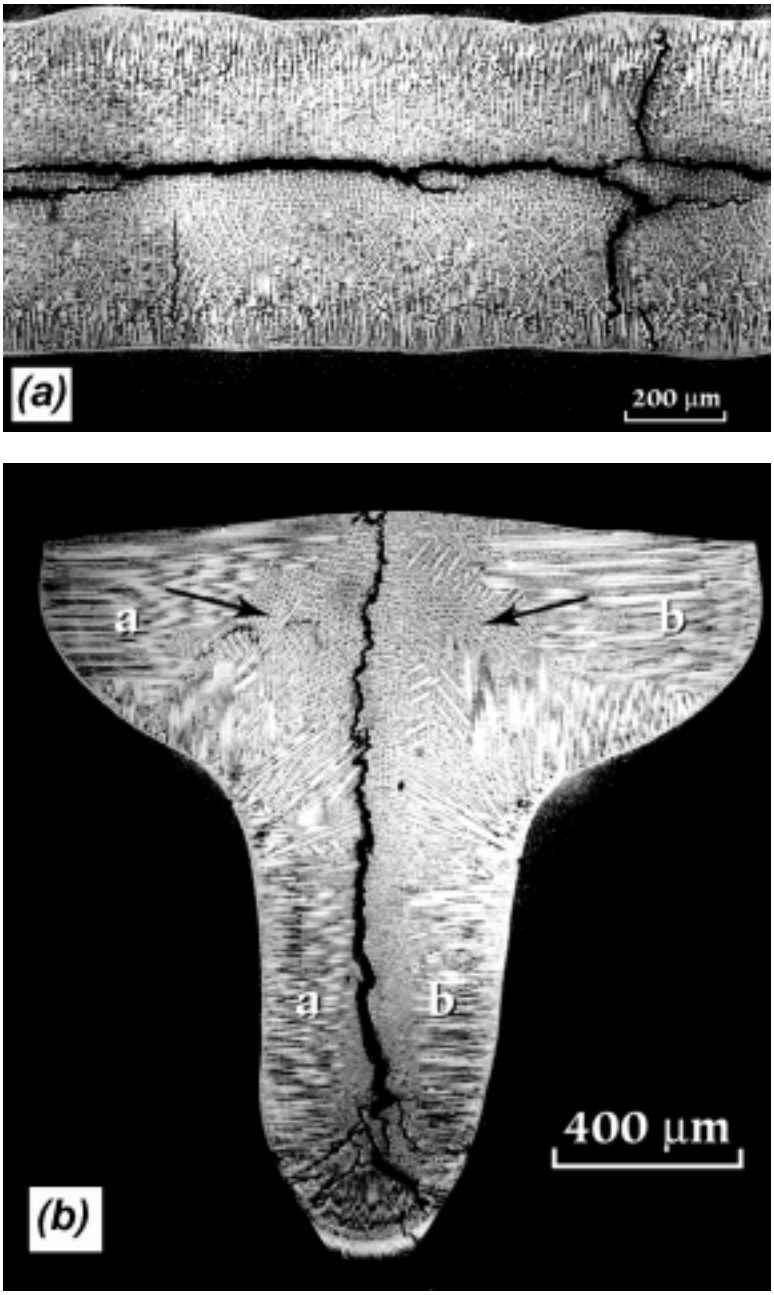

Fig. 1 Optical macrograph of PWA1480 alloy single crystal electron beam weld (*a*) from top surface macroscopic view and (*b*) from transverse section of the weld

An extensive microstructural analysis using scanning electron microscopy (SEM) revealed the dendritic nature of the crack surface, indicating that these cracks are hot-cracks or solidification cracks. Figure 2 shows an SEM photomicrograph of the cracked surface.

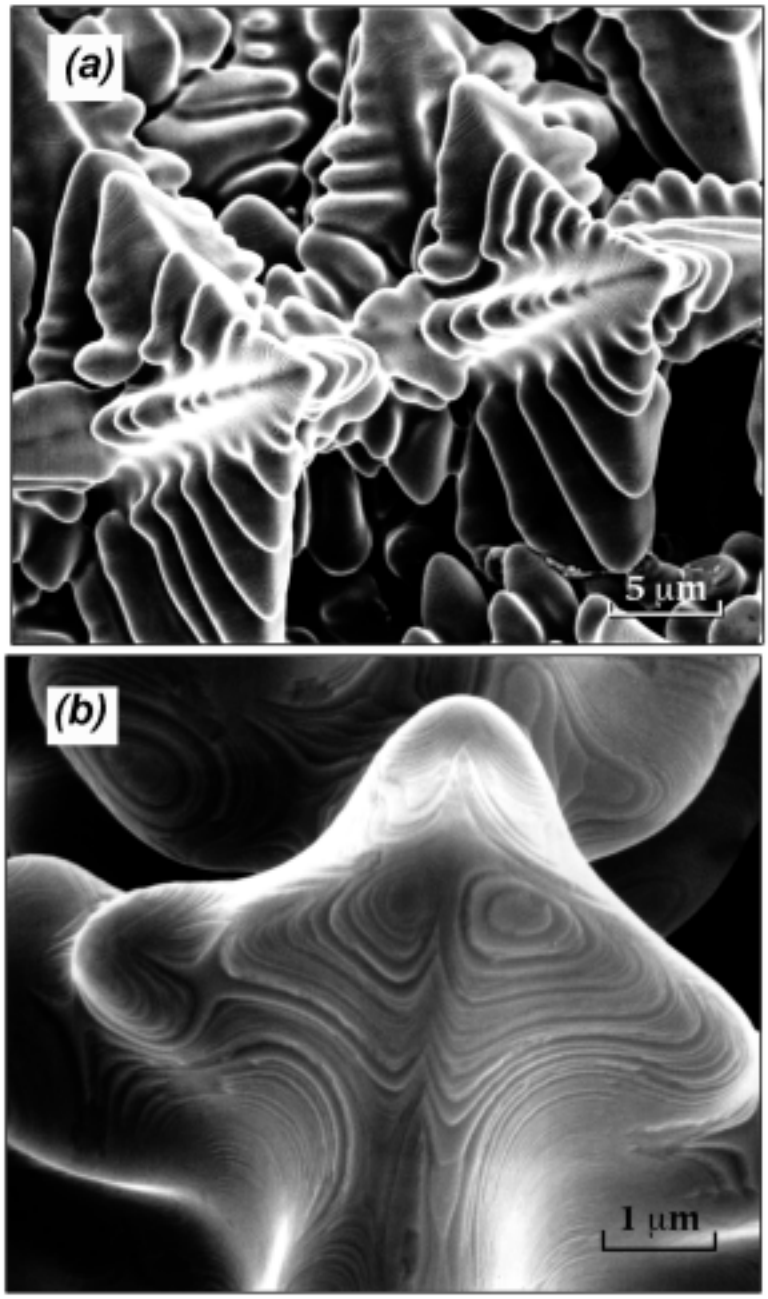

Fig. 2 Scanning electron micrographs showing dendritic features on weld hot crack surface (*a*) at low magnification and (*b*) at high magnification.

The weld orientation had no apparent effect on the cracking tendency. In spite of the observed weld cracking over a range of welding parameters, successful welds were

made at low welding speeds with preheat. Welds without cracks were produced at welding speeds of 4.2 and 6.3 mm/s with a preheat of 500°C.

Laser Welding

Laser welds were made on the crystal discs along the [100] crystallographic direction in (100) plane. The welding speed ranged from 2.1 to 25 mm/s. The laser welds also showed a severe cracking tendency. Figures 3 shows photomicrographs of the top and transverse surface of the laser welds.

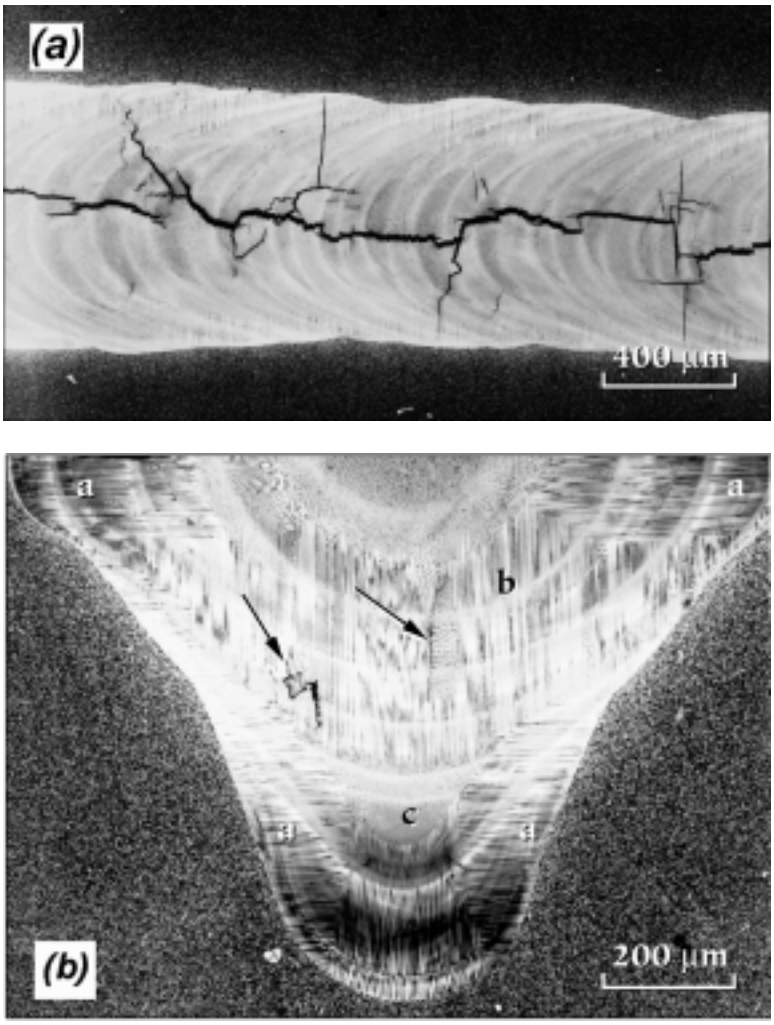

Fig. 3 Macroscopic view of PWA1480 single crystal laser welds carried out at 12.6 mm/s (*a*) top surface and (*b*) transverse section. The regions marked as "a", "b", and "c" in the micrographs correspond to different growth directions.

For all the speeds and pulses investigated, the welds contained centerline cracks with side branches. Extensive cracking is clearly evident in the top surface sections. As observed for EB welds, a preheat of 500°C prevented cracking for welds made at low welding speeds and high pulse rates. However, even with the preheat, cracks appeared

in the welds made at low speeds and low pulse rates. The reasons for this complex behavior are not yet understood.

Microstructure

Base Metal

The overall microstructure of the PWA-1480 single-crystal alloy contained coarse, cuboidal $L1_2$- ordered γ' precipitates uniformly distributed in a γ matrix. The microstructural analysis of the base metal revealed well-aligned primary dendrites with an interdendritic γ/γ' eutectic. This is in agreement with previous published literature [15].

Fusion Zone

The development of the fusion-zone grain structure in a weld is primarily controlled by the base metal grain structure and the welding conditions. The base metal acts as a substrate upon which growth of the solid phase occurs. Both crystallographic effects and welding conditions can influence the development of microstructures in the fusion zone. Specifically, crystallographic effects will influence grain growth by favoring growth along particular crystallographic directions. For cubic metals, such as the nickel-base superalloys considered in this paper, the easy growth directions are the <100> directions. Conditions for growth are optimum when one of the easy growth directions coincides with the heat-flow direction.

The situation for welds made with single crystals is quite different. Since there are no multiple grains available, one has to deal with the selection and epitaxial growth of dendrites at the fusion boundaries for a single grain with one orientation. Significant advances have been made in recent years in determining the dendrite-growth selection process for single-crystals (9-12). Figure 1 shows transverse and top-surface micrographs of a PWA-1480 single-crystal EB weld made on the (001) plane along the [100] direction at a speed of 12.6 mm/s. The dendrites are branched in these welds. This is expected because of the extensive alloying and the associated constitutional under-cooling effects. These factors promote branching of the dendrites (13,16).

From the photomicrographs, both well-aligned and randomly oriented dendrites are visible. The alignment is more clearly visible in the transverse section. These dendrites grow parallel to the three <100> crystallographic directions with the epitaxial growth of dendrites occurring from the base crystal. For example, Figure 1(*b*) shows [010] and $[0\bar{1}0]$ dendrites at the top and bottom half of the weld in the regions marked (a) and (b). The welds in PWA-1480 do not maintain single crystallinity. There is evidence of extensive stray crystal formation in the center of the weld. A detailed discussion of the microstructural evolution in this single- crystal alloy is presented elsewhere (13).

As in the case of the EB welds, the development of microstructural features in the laser weld within the fusion zone is controlled by epitaxial growth of dendrites from the single-crystal base metal and, depending on the pool shape, selection of one of the <100> variants of the dendrites takes place. Figure 3(*b*) shows a transverse photomicrograph of a weld made on a PWA-1480 single-crystal disc with a (011) face and along the [100] direction at 12.6 mm/s. The microstructure shows a predominant growth of [010] and [0$\bar{1}$0] dendrites along the sides at the top and bottom of the weld in the regions marked (a). Also, extensive growth of [001] dendrites is observed in the center portion of the weld in the regions marked (b). In addition, evidence of [100] dendrites is observed in region (c). From Figure 3(*b*), it is clear that the weld also contains stray grains at the top of the weld and, in a few selected areas within the weld (as shown by the arrows). These grains are generally located in the center of the weld and play a critical role in promoting hot-cracks in the weld as discussed later.

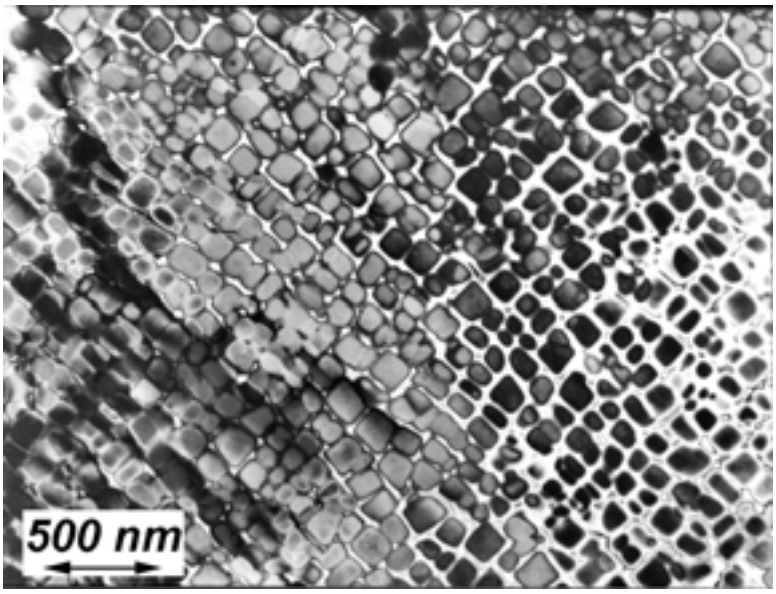

Fig. 4. Transmission electron micrograph of the PWA-1480 weld metal region in the as-welded condition showing the fine γ' precipitate distribution within the core of the γ dendrite.

A detailed characterization of the fusion zone using atom-probe field-ion microscopy (APFIM) revealed a number of interesting features. These features specifically pertain to alloying element partitioning between γ and fine γ' formed during solid state transformation. As the weld metal cools below the solidus temperature, the γ phase decomposes into a mixture of γ and γ' phases. A fine distribution of γ' precipitates within the γ phase was observed as shown in Figure 4. It was speculated that rapid cooling conditions may lead to interfacial segregation at γ/γ' interfaces and nonequilibrium compositions of γ and γ' phases. This speculation was investigated with atom probe field ion microscopy. A field-ion image of the PWA-1480 weld in the as-welded condition is shown in Figure 5.

The image shows the darkly imaging γ phase and the brightly-imaging γ' precipitates. The atom-probe composition profile obtained from this sample showed that most of the aluminum, titanium, and tantalum partitions to the γ' phase. This is in agreement with published results (15, 17). The elements cobalt, tungsten, and chromium partition to the γ matrix. The concentration profiles show no segregation at the γ / γ' interfaces. It is noteworthy that the alloying elements continuously partition between the γ / γ' phases despite the rapid cooling conditions. The heavy elements such as tantalum and tungsten, which are expected to diffuse slowly, were also found to partition during weld cooling. Further work is necessary to characterize the segregation and nonequilibrium partitioning characteristics in the welds with different cooling conditions to evaluate the effect of process conditions. It is also desirable to monitor the changes in the partitioning behavior in these welds on post-weld heat treatment and during thermal aging under service conditions.

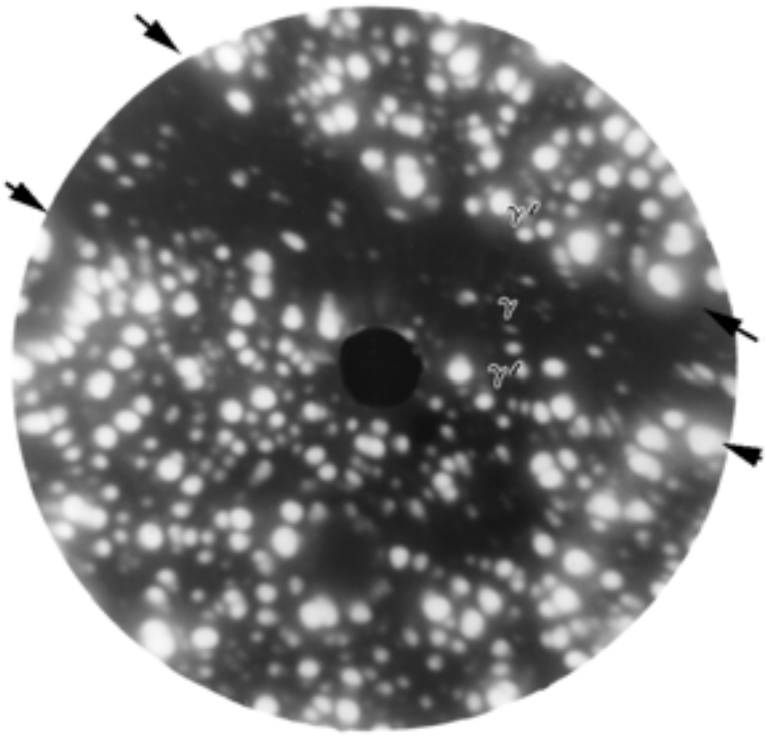

Fig. 5 Field ion micrograph of γ matrix (dark region), γ´ precipitates (bright) and the γ–γ´ interfaces. The arrows show the interface between γ and γ´ phases.

Hot-Cracking

Hot cracking during welding has been studied experimentally and different manifestations of hot- cracking phenomena during welding are (18-22):

1. solidification cracking,

2. liquation cracking in the HAZ, and

3. a combination of the above two.

Nickel-base superalloys are prone to some, or all, of these types of hot-cracks. The type that is of interest to welding the PWA-1480 alloy, however, is solidification cracking. According to Borland (23) the tendency of an alloy to form solidification cracks is directly related to the difference between the solidus and liquidus temperatures of the alloy. Thus, alloys having extended solidification temperature ranges are more susceptible to fusion-zone solidification cracking than are alloys which solidify over a narrow temperature range. In the PWA-1480 alloy, the liquidus temperature is 1588 K, and the eutectic reaction extends the effective solidus temperature down to ≈ 1505 K, resulting in a solidification temperature range of ~ 83ºC [14]. The presence of the eutectic during the last stages of solidification, in combination with the thermal stresses that develop during welding and large solidification range, promotes solidification cracks in this alloy. The SEM photomicrograph of the crack surface shown in Figure 2 demonstrates the dendritic nature of the crack surface, which is evidence that these cracks are solidification cracks.

Another interesting phenomenon associated with the observed weld cracks is the presence of stray crystals in the welds and their role in promoting these cracks. In the present investigation, the cracks were often associated with these stray crystals as shown in Figures 1 and 3. This is further illustrated in Figure 6 for a laser weld shown at high magnification.

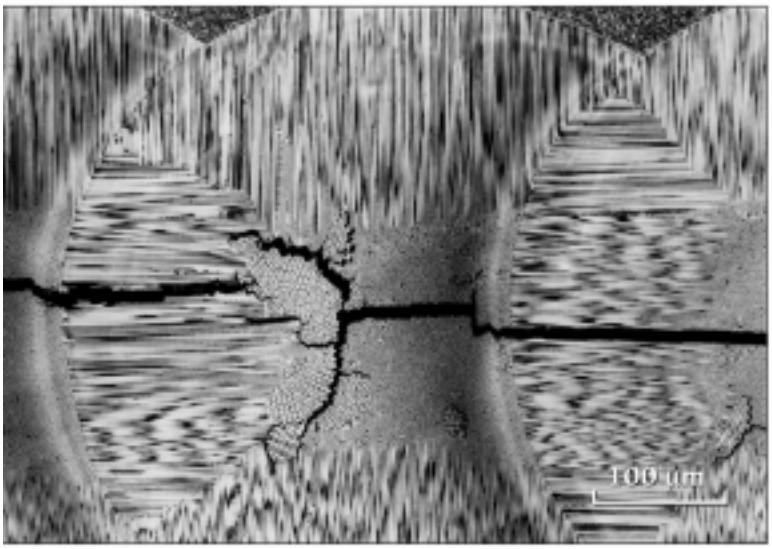

Fig. 6 Microstructure of pulsed laser weld showing dendrite growth pattern within weld and the presence of stray grains in center of the weld associated with hot-cracks.

The stray crystals are misoriented grains within the weld with distinct high-angle grain boundaries. Since there are only a few of these grains, the total high-angle grain boundary area is small. In the presence of low melting eutectic liquid during solidification, the small amount of grain boundary area leads to complete wetting of these high-angle grain boundaries. With the above microstructures, in the presence of thermal stresses, the tendency for weld cracking will be enhanced. The cracking in the presence of a few stray crystals may be eliminated by reducing stresses during welding. This indeed was the case for welds made with a large preheat, which resulted in low thermal stresses. The reasons for less tendency to crack in high-pulse rates is still not clear.

Computational Thermodynamics and Modeling

To illustrate the microstructural development in the PWA-1480 alloy, the phase changes in a Ni-10Cr-5Co-5Al-1.5Ti (wt.%) alloy, as it solidifies from the liquid state, were calculated using computational thermodynamic software [24, 25]. The calculations ignored the effect of Ta and W due to the software limitations. According to the equilibrium phase diagram, the solidification to γ starts at 1676 K and is completed at 1664 K.[†] Since the weld cooling conditions are far from equilibrium, this may not be a proper representation of the weld solidification. The variations in the compositions of the γ matrix and liquid phase during non-equilibrium solidification in the same alloy (assuming Scheil's model) were calculated using the ThermoCalc™ software. The results are compared in Fig. 7.

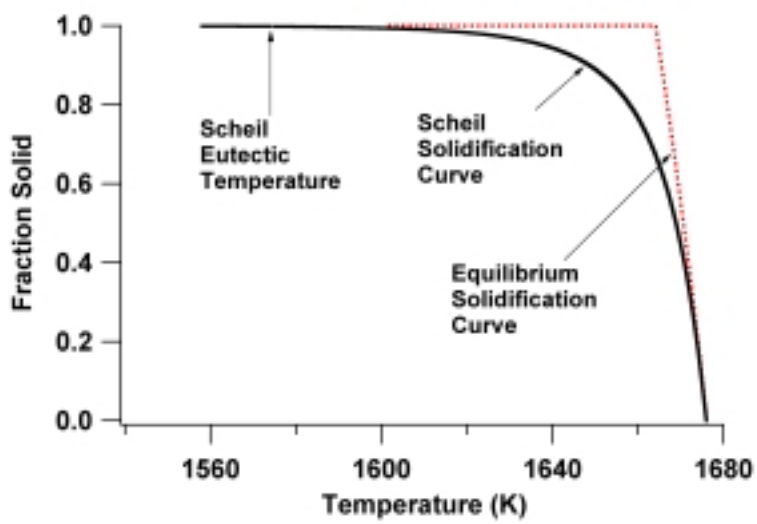

Fig. 7. Calculated solidification curves with equilibrium assumption and the with scheil assumption for an alloy Ni-10Cr-5Co-5Al-1.5Ti (wt.%).

[†] This temperature range is different from the experimental measurement [14], because the calculation cannot consider the effects of Ta and W and also the kinetic effects.

The calculations indicate that the solidus temperature will be lowered by 105 K to 1559 K. This result has large implications on the tendency of these alloys to exhibit solidification cracking during welding. ThermoCalc™ calculations also suggested that the final liquid, due to solute enrichment, might undergo a eutectic reaction at 1574 K. The observation of large γ' precipitates interlaced with films of the γ phase supports this mode of solidification for the weld [14]. Further work is necessary to extend the thermodynamic calculations to consideration of other elements to predict the partitioning characteristics of γ and γ' phases during continuous cooling and thermal aging conditions.

Conclusions

Autogeneous EB and laser welds made on single crystal nickel-base superalloy PWA-1480 showed extensive cracking. The cracks were found to be solidification cracks formed during welding due to the presence of low melting eutectic. However, successful welds were produced in a very narrow range of welding parameters with 500°C preheat.

In both EB and laser welds, several unique microstructural features were identified. The dendrite selection process and the final growth pattern were affected by the pool shape and the initial crystal orientation. The welds contained extensive amounts of misoriented stray grains in the center of the welds. The formation of these stray crystals can be attributed to both thermal and constitutional undercooling effects. These stray grains play a critical role in promoting cracks in the welds.

The APFIM investigations revealed no γ / γ' interfacial segregation. The compositions of the γ / γ' phases were found to be similar to those of the base metal.

Computational thermodynamic methods allow for estimation of the freezing range and phases that form during weld solidification. This information can be used to evaluate the tendency for solidification cracking.

Acknowledgement

The authors would like to thank Dr. Robert Schaefer of United Technologies, Inc. for providing single crystal material that was used in this investigation. This research was sponsored by the Division of Materials Sciences and Engineering, U.S. Department of Energy, under DE-AC05-00OR22725 with UT-Battelle, LLC. The authors also thank Q. Han and J. F. King for reviewing the paper.

References

1. F.L. VerSnyder and B.J. Piearcey: *SAE J.*, 1966, **74**, 36-43.

2. F.L. VerSnyder and M.E. Shank: *Mater. Sci. Engr.*, 1970, **6**, 213-240.

3. M. Gell and D.N. Duhl: 'Advanced High Temperature Alloys', 41-49; 1985. Materials Park, OH, American Society for Metals.

4. M. Gell, D.M. Duhl, and A.F. Giames: 'The Development of Single Crystal Superalloy Turbine Blades,' in Proc. 4th International Symposium, September 1980, 205-214.

5. K.C. Antony and G.W. Goward: 'Aircraft Gas Turbine Blade and Vane Repair,' in Superalloys, (ed. S. Reichman, D.N. Duhl, G. Maler, S. Antolovich, and C. Lund), 1988, 745; Warrendale, PA, The Metallurgical Society

6. J. Liburdi and P. Lowden: 'Repair standards for aero and industrial turbine blades,' Report No. 89-GT-244, International Gas Turbine Institute, American Society of Mechanical Engineers, New York, 1989.

7. P.C. Patnaik, M.R. Pishva, J.E. Elder, W. Doswell, and R. Thamburaj: 'Repair and life extension of titanium alloy for blades in aircraft-gas turbines', Report No. 89-GT-166, International Gas Turbine Institute, American Society of Mechanical Engineers, New York, 1989.

8. T.E. Doyle, D.F. Busch, and T.J. Johnson: in Proc. Conf. '28th National SAMPE Symposium, Covina, California, April 1983

9. M. Rappaz, S.A. David, J.M. Vitek, and L.A. Boatner: *Metall. Trans.*, 1989, **20A,** 1125-1137.

10. M. Rappez, S.A. David, J.M. Vitek, and L.A. Boatner: *Metall. Trans.*, 1990, **21A,** 1767-1782.

11. S.A. David, J.M. Vitek, M. Rappez, and L.A. Boatner: *Metall. Trans.*, 1990, **21A,** 1753-1766.

12. S.A. David, J.M. Vitek, L.A. Boatner, and M. Rappaz: *Mater. Sci. Technol.*, 1995, **11**, 39.

13. J.M. Vitek, S.A. David and L. A. Boatner: *Science and Technology of Welding and Joining*, 1997, **2**, 109.

14. S. A. David, J. M. Vitek, S. S. Babu, L. A. Boatner, and R. W. Reed, *Science and Technology of Welding and Joining*, 1997, **2**, 79.

15. M.K. Miller, R. Jagaram, L.S. Lin, and A.D. Cetel: *Appl. Surf. Sci.*, 1991, **76/77**, 172-176.

16. J. Gayda, R.L. Dershfield, and T.P. Gabb: *Scr. Metall. Mater.* 1991, **25,** 2589-2594

17. D. Blavette, P. Caron, and T. Khan: *Scripta Metall.*, 1986, **20**, 1395

18. T. Ogawa: *Weld. Intl.*, 1991, **5**, 931-935.

19. P.P. Puzak, W.R. Apblett, and W.S. Pellini, *Weld. J.*, 1956, **35**(1), 96s-175s.

20. W.R. Apblett, and W.S. Pellini: *Weld. J.*, 1954, **33**(2), 83s-90s.

21. J.C. Borland: *British Weld. J.*, 1960, **7**, 558-59.

22. F.C. Hull: *Weld. J.*, 1967, **46**, 399s-409s.

23. J. C. Borland: *British Weld. J.*, 1960, **7**, 508-512.

24. B. Sundman, B. Jansson, and J. O. Andersson, *Calphad*, 1985, **9**, 153-190.

25. N. Saunders, "Ni-Fe data information", Thermotech Ltd., Surrey Technology Center, Guidford, Surrey, GU2 5YG, UK, 1999.